Ionics (2020) 26:6359–6369
https://doi.org/10.1007/s11581-020-03749-5

ORIGINAL PAPER

Cu_2O/MoS_2 composites: a novel photocatalyst for photocatalytic degradation of organic dyes under visible light

Xuexin Zhang[1] · Mingzhu Xia[1] · Fengyun Wang[1] · Wu Lei[1]

Received: 18 January 2020 / Revised: 2 August 2020 / Accepted: 22 August 2020 / Published online: 31 August 2020

Abstract

The novel nanocomposite Cu_2O/MoS_2-12 was synthesized by a simple two-step method. Cu_2O nanospheres grow on the surface of MoS_2 nanoflowers and have high photocatalytic activity. X-ray diffraction (XRD), scanning electron microscopy (SEM), transmission electron microscope (TEM) X-ray photoelectron spectroscopy (XPS), ultraviolet-visible light (UV-vis) photoluminescence (PL) spectroscopy, UV-vis diffuse reflection (UV-DRS), and electrochemical impedance (EIS) were used to study the structure and properties of the samples. The photocatalytic properties of the materials were evaluated by degrading methyl orange (MO) under visible light. The results show that CM-12 can completely degrade MO in 30 min, and the pseudo-first-order kinetic constant of degradation is 8.76 times that of pure Cu_2O, which can be attributed to the composite material that can greatly reduce the recombination rate of photogenerated electrons and holes, and it has good stability. After repeated use for 5 times, the degradation rate can still reach 40%. Through experiments and theoretical results, a possible photocatalytic mechanism is proposed. To the best of our knowledge, this work was the first example of combining MoS_2 with Cu_2O and applying it to photocatalytic degradation of organic pollutants. It was beneficial for developing new photocatalysts and improving the catalytic performance of conventional photocatalysts.

Keywords Cu_2O · Methyl orange · MoS_2 · Nanocomposite · Photocatalyst

Introduction

In recent years, the organic azo dye methyl orange (MO) has been widely used in textile, paper, leather, and other industries due to its bright color. At the same time, some methyl oranges are also left in various wastewaters, causing certain harm to the environment [1]. Therefore, a technology that uses sustainable solar energy to solve current energy and environmental problems (semiconductor photocatalytic technology) has received widespread attention [2–4]. Semiconductor photocatalytic technology decomposes pollutants by generating OH radicals and other oxidizing substances, and finally mineralizes them into harmless carbon dioxide and water [5–7].

✉ Mingzhu Xia
xiamzh196808@njust.edu.cn

✉ Fengyun Wang
wangfy@njust.edu.cn

[1] School of Chemical Engineering, Nanjing University of Science and Technology, Nanjing 210094, China

Cu_2O is a photocatalyst with a bandgap of about 2.0 eV [8]. As a semiconductor photocatalytic material, it has the advantages of being non-toxic, easy to obtain raw materials, and degradable organic substances under visible light [9]. So far, different forms of Cu_2O have been used in photocatalysis, such as cube [10], octahedron [11], and polyhedron [12]. However, the recombination of photogenerated electrons and holes is still an important factor leading to the reduction of Cu_2O photocatalytic activity [13]. The above problems can be solved by synthesizing a composite semiconductor material, and the former has made the following efforts. Including synthesis of Cu_2O/ZnO [14], Cu_2O/CeO_2 [15], and Cu_2O–TiO_2 [16], all effectively improve photocatalytic activity.

Over the last decade, the metal sulfide molybdenum disulfide (MoS_2) has received wide attention due to its high fluidity carriers and excellent light absorption properties [17]. MoS_2 also has a two-dimensional layered structure similar to graphene, with a high surface area and strong surface adsorption capacity, and is a potential co-catalyst for photocatalytic reactions [18]. These structures and optical properties are advantageous in the photocatalytic process. However, it also has disadvantages, such as insufficient charge separation and poor

charge mobility, which can affect its photocatalytic ability. Therefore, it is necessary to overcome these disadvantages in order to improve the photocatalytic ability [19]. In order to solve the above problems, many efforts have been made by the predecessors, such as composite MoS_2/GO [20], MoS_2/g-C_3N_4 [21], and MoS_2/TiO_2 [22].

Based on the above considerations, a simple two-step method is used to combine Cu_2O and MoS_2, and through the calculation of valence band and conduction band, they have matching bandgaps, and it is expected that the effect of improving the electron-hole separation ability and thus the photocatalytic activity can be achieved. Multiple characterizations also prove this, and according to previous reports, there are few reports on the use of the combination of the two to degrade organic matter.

Experimental section

Raw materials

Copper nitrate hydrate ($Cu(NO_3)_2{\cdot}3H_2O$), hydrazine hydrate ($N_2H_4{\cdot}H_2O$, 85%), and thiourea (CH_4N_2S) were purchased from Chengdu Kelon Chemical Reagent Factory, Sodium molybdate($Na_2MoO_4{\cdot}2H_2O$) Tianjin Chemical Reagent Fourth Factory, Citric acid monohydrate($C_6H_8O_7{\cdot}H_2O$) Nanjing Chemical Reagent Co., Ltd.

All of these reagents were of analytical grade and used without further purification.

Synthesis of Cu_2O/MoS_2 composites

Synthesis of layered MoS_2 nanoflowers

Layered molybdenum disulfide synthesized by the hydrothermal method [23], 0.5 g of $Na_2MoO_4{\cdot}2H_2O$ and 0.7 g of NH_2CSNH_2 were mixed together with 0.47 of citric acid in 70 mL distilled water termed as solution I. The solution I was magnetically stirred for 30 min, placed in a 100 ml polytetrafluoroethylene autoclave, and placed in an oven at 200 °C for 24 h. After the reaction was completed, it was washed with distilled water and absolute ethanol several times, and filtered to obtain a black solid, which was placed in an oven at 60 °C for 12 h for use.

Synthesis of Cu_2O/MoS_2 composites

As shown in Fig. 1, Cu_2O/MoS_2 were prepared through a two-step reduction method by $N_2H_4{\cdot}H_2O$ [24]. (1) 30 mg of the obtained molybdenum disulfide was mixed with 50 ml of deionized water and ultrasonically dispersed for 1 h to obtain a molybdenum disulfide solution (0.6 mg/ml). (2) 50 mg of $Cu(NO_3)_2{\cdot}3H_2O$ and 12 ml of 0.6 mg/ml of molybdenum disulfide solution was mixed with 50 ml of distilled water, and magnetically stirred for 1 h. Due to electrostatic adsorption, Cu^{2+} was adsorbed on the surface of MoS_2. (3) After 1 h, 1 ml of $N_2H_4{\cdot}H_2O$ (0.5 M) was added and stirred for 5 min. After the completion of the stirring, 1.5 ml of $N_2H_4{\cdot}H_2O$ (0.5 M) was added. Cu^{2+} adsorbed on the surface of MoS_2 was reduced to Cu_2O. After the reaction was complete, it was washed with distilled water and absolute ethanol, filtered, and dried in an oven at 60 °C for 6 h.

By adding different concentrations of MoS_2 solution (4 ml, 8 ml, 12 ml, 16 ml), the Cu_2O and MoS_2 are composited to obtain Cu_2O/MoS_2 complexes CM-4, CM-8, CM-12, CM-16 with different ratios. The relative contents of MoS_2 in the corresponding composites were 6.4%, 12.1%, 17.1%, and 21.5%, respectively. The synthesis method of cuprous oxide is the same, except that molybdenum disulfide is not added.

Characterization

The structure and composition of the composite were investigated by using a German Bruker D8 X-ray diffractometer (XRD) with K_α radiation of Cu ($\lambda = 1.5418$). The UV-visible DRS spectra (Thermo Fisher Scientific) of the measured samples were based on barium sulfate. The insight geometry of the sample was recorded by SEM (Quanta 250F, USA). The sample TEM was measured by FEI Tecnai G2 F20. The UV-vis diffuse reflectance absorption spectrum was measured using an ultraviolet spectrometer of EV220 (American Thermo Fisher Scientific Co., Ltd.). The PL spectra were tested on a FL3-TCSPC fluorescence spectrophotometer. XPS of the material was attained by disbursing an RBD upgraded PHI-5000C ESCA system with Mg Kα (1486.6 eV) radiation.

Photocatalysis experiments

A 500 W xenon lamp (with UV filter $\lambda > 420$ nm) was used as a visible light source to degrade the organic dye methyl orange (MO). During each experiment, 10 mg of photocatalyst was mixed with 50 ml of MO at a concentration of 20 mg/L. The dark agitation was carried out for 30 min before the start of visible light degradation. After the adsorption equilibrium, the photocatalytic degradation was started and about 3 ml of the suspension was collected every 5 min. After centrifugation, the supernatant was analyzed by UV-visible spectrophotometer. The maximum absorption wavelength of organic dye MO was 464 nm.

Photochemical measurement

Electrochemical impedance spectroscopy (EIS) measurements were performed on a CHI660D electrochemical workstation (Shanghai Chenhua Instrument Co., Ltd., China) to

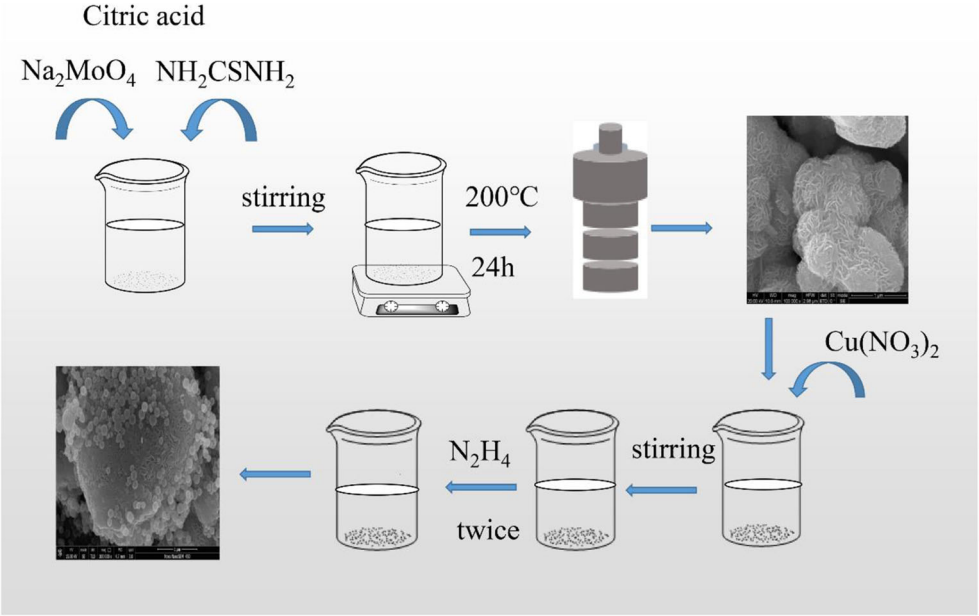

Fig. 1 Schematic diagram of the synthetic process of CM-12 composite photocatalyst

prepare a photoelectrode, and 1 mg of the photocatalyst sample was ultrasonically mixed with 1 ml of ethanol. The 6 μL suspension was dip-coated onto a 2 cm^2 FTO glass electrode, then dried overnight and a saturated calomel electrode (SCE) was used as a reference electrode. Electrochemical impedance spectroscopy (EIS) was performed at an open circuit potential at a frequency of 0.1 to 10^6 Hz, and all experiments were performed in a solution containing 0.5 mM $[Fe(CN)]^{3-/4-}$ in KCl (0.1 M) at room temperature.

Results and discussion

Structure and morphological characterization of Cu_2O/MoS_2 nanocomposites

The crystal phase and composition of the synthesized binary composite sample were studied by XRD analysis. It was very consistent to study the crystal structure of binary composites by XRD. All characteristic peaks were identified, and all peaks for pure were described as hexagonal (PDF #37-1492). The weak peaks in Fig. 2 indicate that the crystallinity was poor MoS_2, and the main peaks were indexed as (002) (100) at 2θ of 13.8°, 32.7°. No other impurity peaks indicated that pure MoS_2 was synthesized. In the diffraction patterns of CM-4 and CM-8, there was no obvious MoS_2 diffraction peak, probably because the amount of MoS_2 was small. As the amount of MoS_2 increases, the characteristic peak of MoS_2 with 2θ of 13.7° (002) could be seen in CM-12 and CM-16. The 2θ of 36.4° and 42.3° could be marked as (111) (200) belongs to Cu_2O (PDF#34-1354). Without other peaks, the composite Cu_2O/MoS_2 was successfully synthesized [25].

SEM was used to study the morphology and size of the material. The SEM image was shown in Fig. 3. Figure 3a and Fig. 3b show pure MoS_2 images at different magnifications. It could be seen that they were nanoflower structures with a size of about one micron. The structure of pure Cu_2O was shown in Fig. 3c. Cu_2O was a nanosphere with a diameter of about 80–200 nm. The SEM image of the composite material CM-12 was shown in Fig. 3d CM-12 used a large-sized MoS_2 nano flower as a carrier and a small-sized Cu_2O structure grown on its surface.

Through TEM and HRTEM to further understand the microstructure, as shown in Fig. 4a, it could be clearly seen that Cu_2O and MoS_2 were combined together. The HETEM image was shown in Fig. 4b, and the crystal plane spacing of 0.247 nm could be observed. It corresponds to the (111) crystal plane of Cu_2O, which was consistent with what was said in the article [26]. The 0.615 nm corresponds to the (002) crystal plane of MoS_2. TEM results further confirmed the formation of the complex.

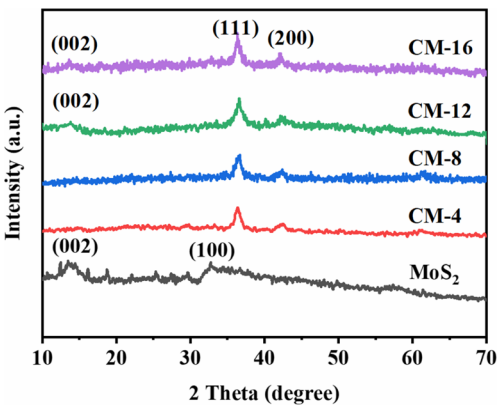

Fig. 2 XRD patterns of MoS_2 and Cu_2O/MoS_2 composites with different ratios

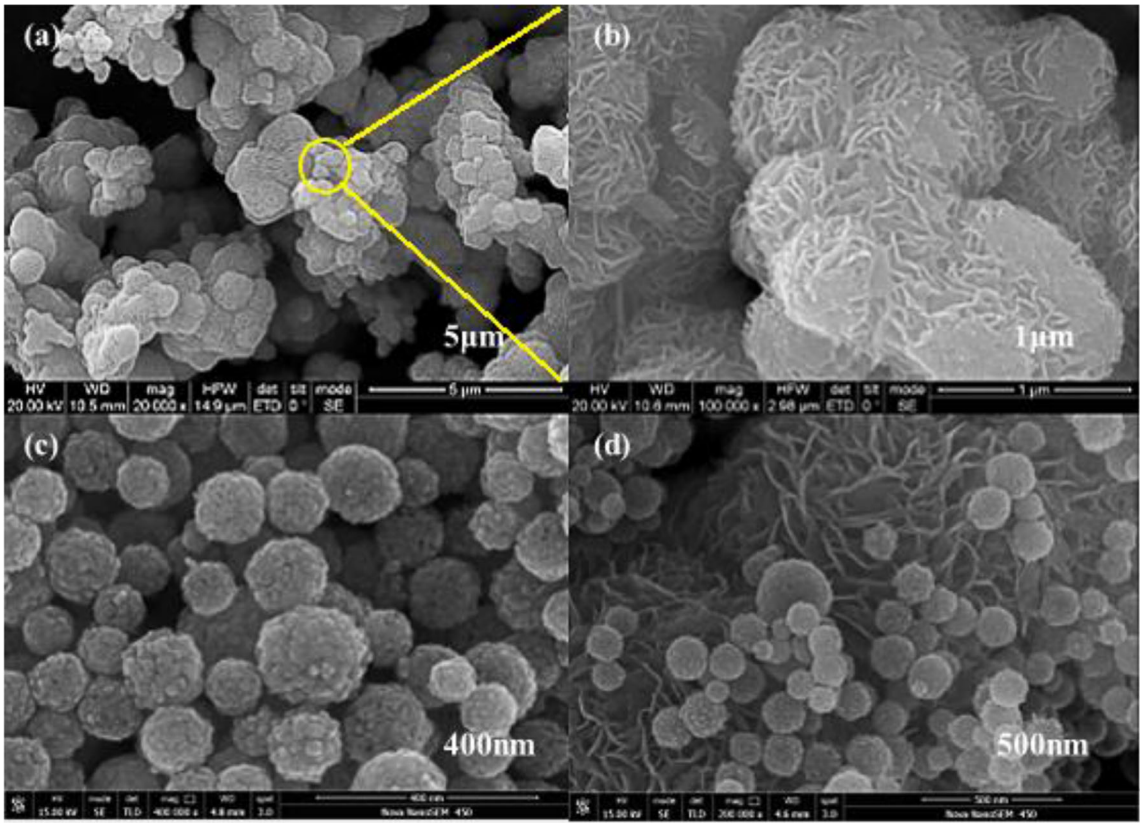

Fig. 3 SEM image of photocatalyst (**a**) and **b** pure MoS_2, **c** pure Cu_2O, **d** composite CM-12

The elemental composition was identified by XPS, and the binding energy obtained in XPS analysis was corrected by setting C1s to 284.8 eV while the sample was being charged. As shown in Fig. 5, the CM-12 composite showed that the material contains Cu, O, Mo, S, and C. Five elements, of which C comes from the instrument itself. The characteristic peaks of Cu2p at 932.6 and 952.4 eV were shown in Fig. 5a, which were attributed to the binding energies of Cu2p3/2 and Cu2p1/2 [27, 28], respectively, but because the binding energies of Cu2p3/2 and Cu2p1/2 were very close, it was difficult to distinguish between Cu_2O and Cu by XPS features. However, in Fig. 5e, the X-ray-induced Cu LMM Auger spectrum was about 570.0 eV, which proved that the main copper species was Cu_2O [29]. The characteristic peaks of O1s at 530.7 eV and 531.9 eV in Fig. 5b belong to the lattice oxygen and surface adsorption oxygen (O_2 or H_2O) of Cu_2O, respectively [30]. In Fig. 5c, the characteristic peaks of Mo3d at 232.3 eV and 228.9 eV belonged to Mo3d3/2 and Mo3d5/2 [31], while the characteristic peak at 226.4 eV belonged to the characteristic peak of S2s in MoS_2 [32]. As shown in Fig. 5d, it could be clearly seen that the S2p spectrum of MoS_2 consists of peaks of 161.6 and 162.7 eV, which were assigned to S2p3/2 and S2p1/2, respectively [33].

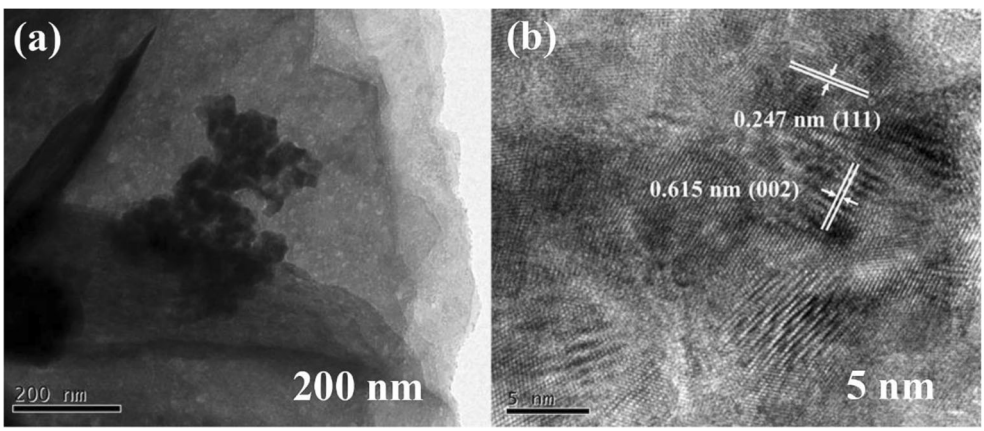

Fig. 4 TEM image (**a**) and HR-TEM image (**b**) of CM-12

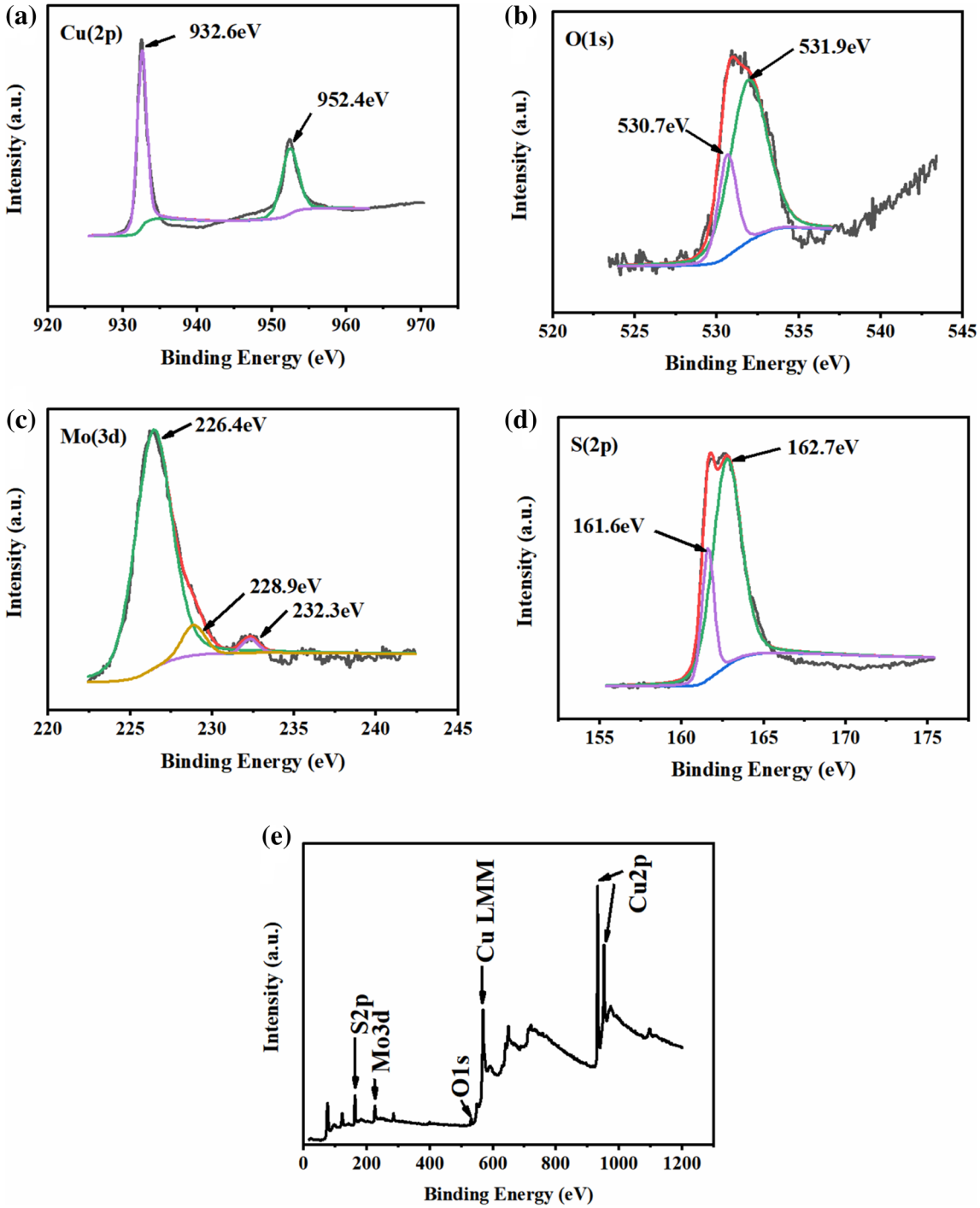

Fig. 5 XPS analysis of the CM-12, **a** Cu(2p); **b** O(1 s); **c** Mo(3d); **d** S(2p) and **e** survey XPS spectrum of CM-12

Photocatalytic activity properties of the Cu_2O/MoS_2 composites

The photocatalytic performance of Cu_2O/MoS_2 was evaluated by degrading methyl orange. First, the photocatalytic properties of composite materials and single materials were compared. The properties of Cu_2O and MoS_2 were measured separately. As can be seen from Fig. 6a, MoS_2 had no degradation effect on methyl orange. In order to study the effects of different MoS_2 doping on the properties of composites, the photocatalytic properties of CM-4, CM-8, CM-12, and CM-16 were tested. The photocatalytic performance of the composite for MO was observed from Fig. 6c. The effect was arranged in ascending order of CM-8, CM-4, CM-16, and CM-12, of which CM-12 had the best degradation effect.

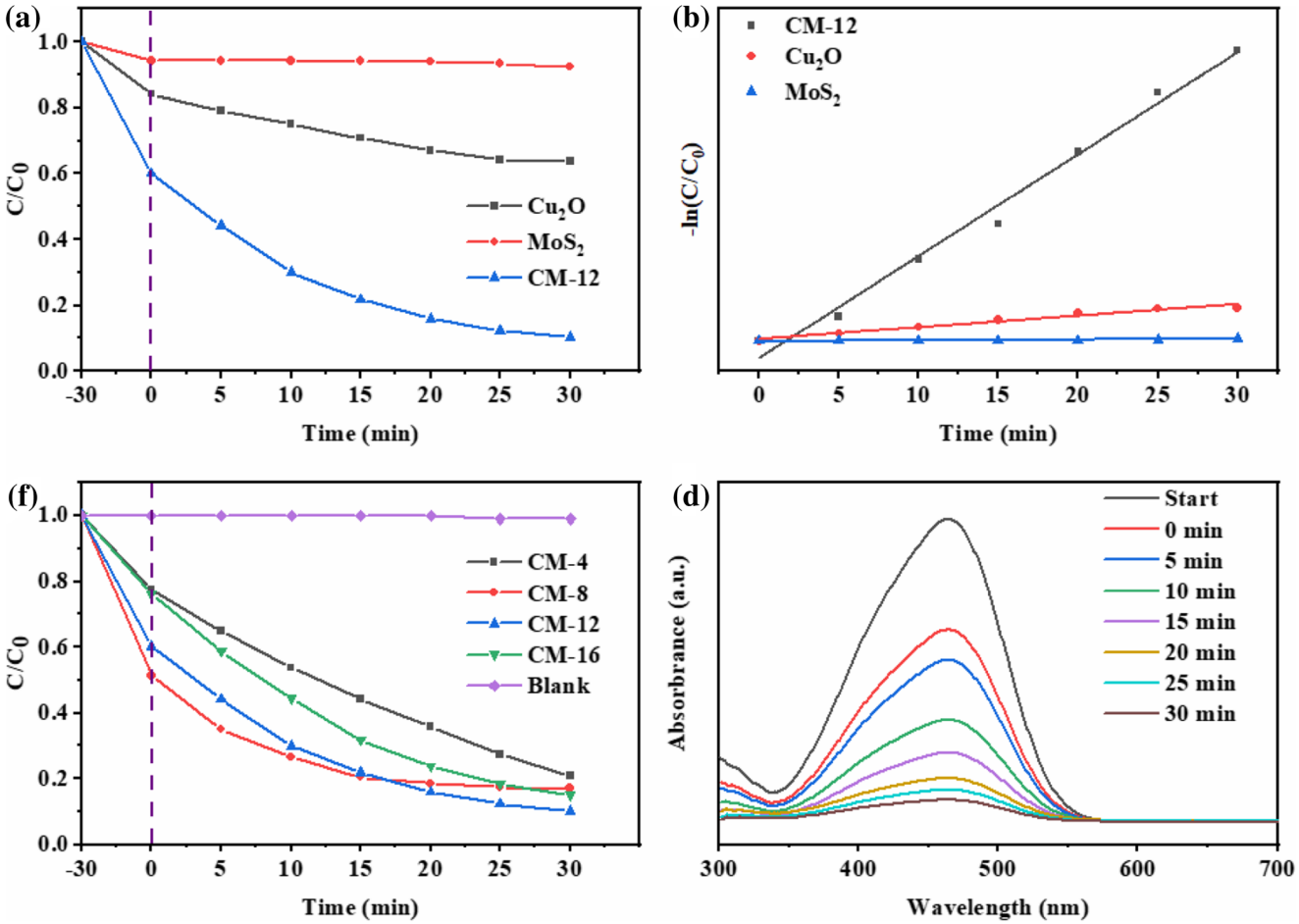

Fig. 6 **a** Photocatalytic degradation of MO with Cu_2O, MoS_2, CM-12. **b** Comparison of pseudo-first-order rate constants (k) for different samples degrading MO under visible light illumination. **c** Degradation of MO using different photocatalysts: molybdenum disulfide in different proportions: CM-4, CM-8, CM-12, CM-16. **d** In the presence of catalyst CM-12, the absorption spectrum of MO varies with the irradiation time

According to the Langmuir-Hinshelwood kinetic model [34], the photocatalytic degradation of MO can be represented by the following pseudo-first-order kinetic Eq. (1):

$$-\ln(C/C_0) = kt \quad (1)$$

where C and C_0 are the concentrations of MO in the solution when the illumination time is t and 0, respectively; k is the pseudo-first-order rate constant; t is time. As shown in Fig. 6b, the k value of pure Cu_2O was 0.00973 min^{-1}, and pure MoS_2 had no degradation of MO. The k value of CM-12 was 8.67 times that of pure Cu_2O, which proved that the photocatalytic performance of the composite was much better than that of a single material. The suitable MoS_2 content (12 ml) can be well combined with Cu_2O nanospheres. The intimate contact interface facilitated the transfer and separation of charge carriers and enhanced photocatalytic activity.

Meanwhile, in order to study the degradation of MO by CM-12, the characteristic absorption peak of MO was observed by UV-Vis spectroscopy (Fig. 6d), and the absorbance at 464 nm gradually decreased with time, indicating that MO was successfully degraded.

Comparing different photocatalysts with the photocatalysts in this article, MO was also degraded. The comparison results were shown in Table 1. It could be seen that CM-12 had a relatively good photocatalytic effect.

Table 1 Comparison of photocatalytic performance of CM-12 and other photocatalysts

Photocatalysts	Amount	Concentration	Time	References
CM-12	0.01 g	20 mg/L(50 ml)	30 min	This article
gC_3N_4/Bi_2WO_6	0.15 g	10 mg/L(50 ml)	30 min	[35]
Co_3O_4- gC_3N_4	0.10 g	10 mg/L(100 ml)	3 h	[36]
$AgBr/Ag_3PO_4$	0.01 g	10 mg/L(50 ml)	50 min	[37]
Ag/TiO_2/biochar	0.01 g	20 mg/L(40 ml)	1 h	[38]
Cu_2O/ZnAl LDH	0.05 g	20 mg/L(50 ml)	7 h	[8]
TiO_2/MoS_2@zeolite	0.125 g	20 mg/L(250 ml)	1 h	[39]
ZnO/Cu_2O	0.20 g	25 mg/L(200 ml)	3 h	[13]
N-TiO_{2-x}@MoS_2	0.05 g	10 mg/L(50 ml)	2 h	[40]

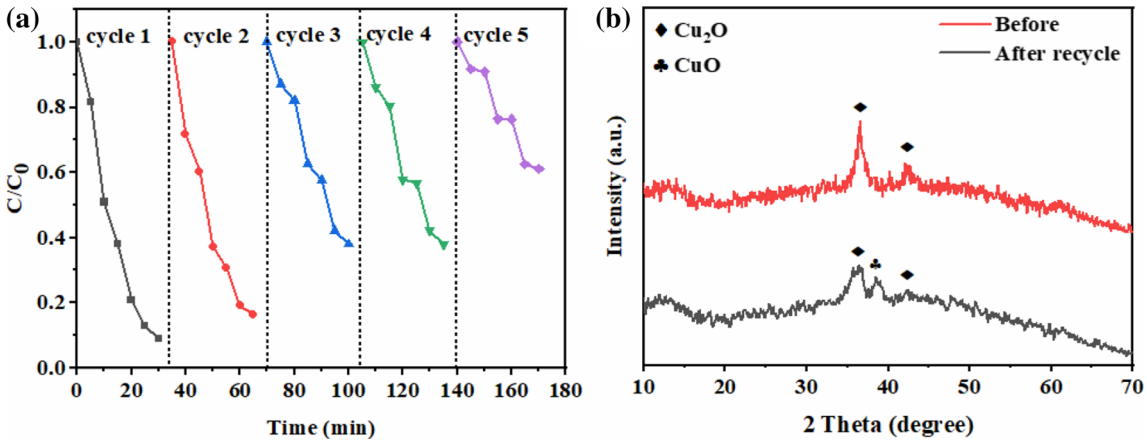

Fig. 7 **a** Photocatalytic degradation curve of CM-12 cycle under visible light irradiation. **b** Comparison of XRD before and after recycling

The stability of photocatalysts

In addition to the photocatalytic degradation effect, the service life of photocatalytic materials is also important in practical applications [41]. We recycle the photocatalyst degradation test. It can be seen from Fig. 7a that the degradation rate was reduced by about 30% after four cycles of recycling, and the degradation rate was reduced by about 50% after repeated use for five times. Comparing the XRD patterns before and after repeated use, the main reason for the decrease in the degradation rate in the later stage may be that some Cu_2O in the composite was oxidized to CuO due to the increase in the number of uses. As can be seen from Fig. 7b, the addition of a new CuO peak in the XRD pattern supports this interpretation. However, the degradation rate after oxidation can still be reached 40%.

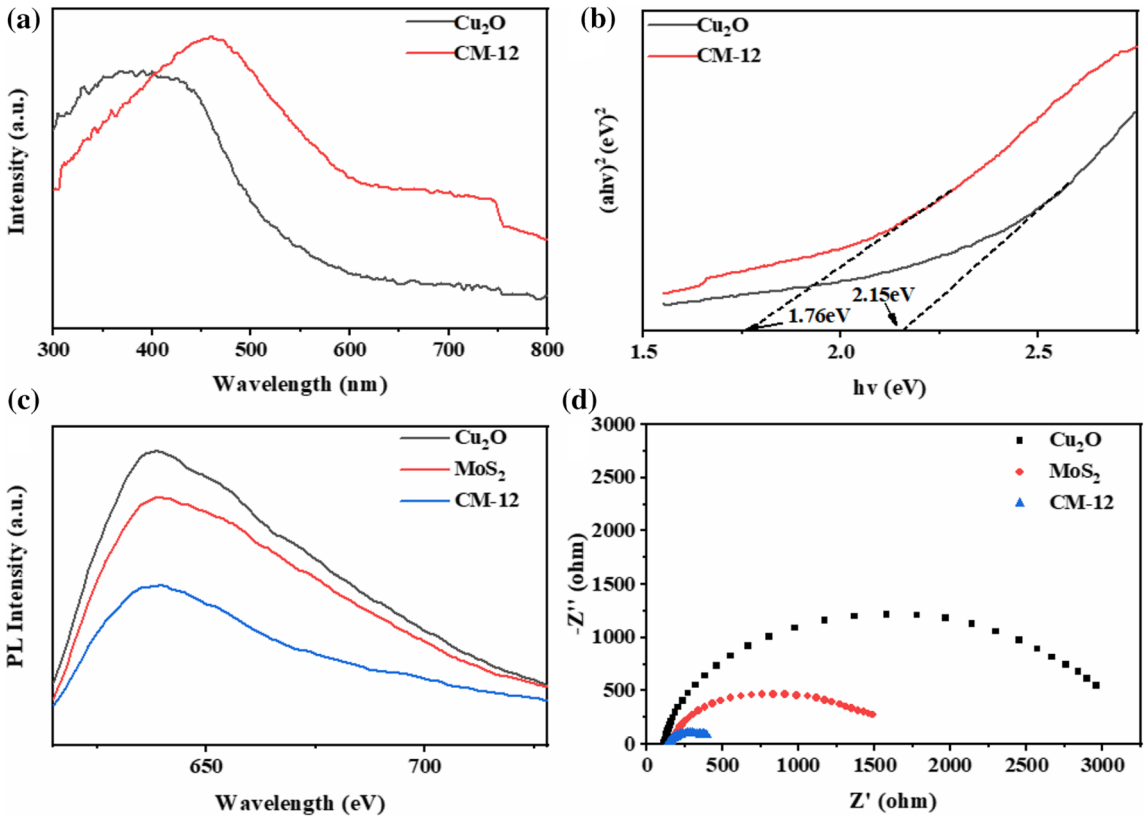

Fig. 8 **a** UV-visible diffuse reflectance absorption spectra of Cu_2O and CM-12. **b** The plot of $(\alpha h\nu)^2$ against $h\nu$ to determine the bandgaps of the Cu_2O and CM-12. **c** Fluorescence spectra of Cu_2O, MoS_2, and CM-12. **d** Electrochemical impedance spectroscopy of Cu_2O, MoS_2, and CM-12

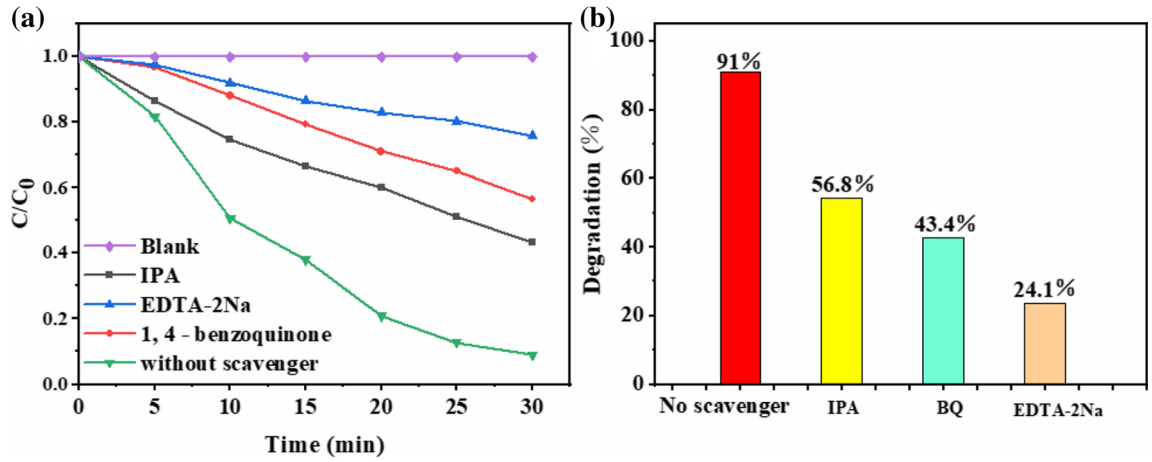

Fig. 9 **a** Different capture agent degradation MO experiments. **b** The corresponding photocatalytic degradation efficiency of composite CM-12 under visible light irradiation

Photocatalytic mechanism for Cu_2O/MoS_2

The energy band characteristics of semiconductors are the key factors determining their photocatalytic activity [34]. Figure 8a shows the UV-DRS spectra of Cu_2O and CM-12. It can be seen that the energy absorption capacity of the composites was enhanced after Cu_2O loading.

In addition, calculate the bandgap of the semiconductor according to the formula:

$$\alpha h\nu = A\left(h\nu - E_g\right)^n \quad (2)$$

Where α, h, ν, A, and Eg represent the absorption coefficient, Planck's constant, optical frequency, constant, and bandgap energy, respectively, and the value of n depends on whether the transition is direct ($n = 0.5$) or indirect ($n = 2$); the bandgap energy is determined by doing a graph of $(\alpha h\nu)^2$ versus hν. It can be concluded from Fig. 8b that the Cu_2O and CM-12 bandgaps were 2.15 eV and 1.76 eV, respectively. As previously reported, PL behavior was closely related to the number of layers of MoS_2, and the bandgap of MoS_2 nanoflowers can be estimated by PL spectroscopy [42].

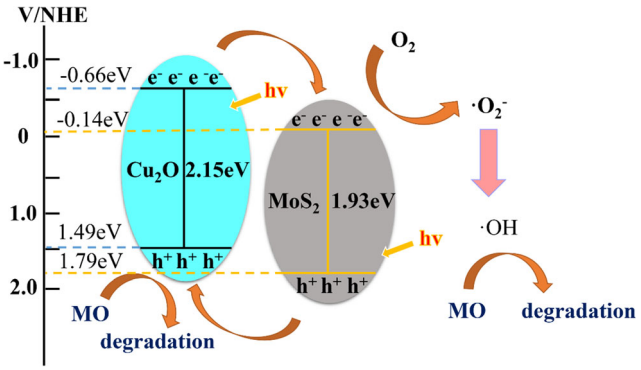

Fig. 10 Photocatalytic mechanism of Cu_2O/MoS_2 nanocomposites

As shown in the PL spectrum of Fig. 8c, the strong peak of MoS_2 at 641 nm corresponds to a bandgap of 1.93 eV. It is reported that PL behavior is closely related to the number of layers of MoS_2, and the bandgap of nano MoS_2 can be estimated by PL spectroscopy [42, 43]. According to the formula, the bandgap of MoS_2 is about 1.93 eV.

$$E = 1240/\lambda \quad (3)$$

The PL emission signal was produced by the recombination of excited electrons and holes, so a lower PL intensity indicates a lower electron-hole recombination rate and a higher photocatalytic activity [44]. Therefore, by comparing the PL spectral intensities, it was possible to compare the charge transfer in different semiconductor materials and the recombination efficiency of photogenerated electron-hole pairs. It can be seen from the figure that with the excitation wavelength of 330 nm, the composite had the smallest fluorescence intensity, that was, the lowest electron-hole recombination rate, which was consistent with the experimental results.

The band edge position of Cu_2O and MoS_2 can be estimated by empirical formula [45],

$$E_{VB} = X - E^C + 0.5E_g \quad (4)$$

$$E_{CB} = E_{VB} - E_g \quad (5)$$

where X is the absolute electronegativity of the semiconductor, and the X values of Cu_2O and MoS_2 are 4.91 and 5.32 eV, respectively. E^C is the free electron energy on the hydrogen scale (about 4.5 eV), E_g is a semiconductor bandgap. It was deduced from the empirical formula that the CB and VB of Cu_2O are − 0.66 and 1.49 eV, respectively, and the CB and VB of MoS_2 were − 0.14 and 1.79 eV, respectively.

Electrochemical impedance spectroscopy (EIS) was used to determine the charge transport capability of the sample under visible light illumination. It was known that a smaller

arc radius means less obstruction to electron-hole transport and a higher efficiency of charge separation [46]. As can be seen from Fig. 8d, the arc radius order of the three materials was Cu_2O and MoS_2 CM-12, respectively. CM-12 was more effective in charge separation, which was consistent with the experimental results. In order to further study the degradation mechanism of photocatalytic degradation of MO by Cu_2O/MoS_2, three different free radical scavengers were added for free radical trapping experiments. That was, isopropanol (IPA), 1,4-benzoquinone(BQ), and disodium EDTA (EDTA-2Na) capture the radical (·OH), superoxide radical ($\cdot O_2^-$) and hole (h^+), respectively [47, 48]. As shown in Fig. 9 a and b, the three scavengers interfered with the degradation of MO compared with no scavenger. IPA, EDTA-2Na, and BQ all have inhibitory effects on the photocatalytic process, and the inhibitory effects are ranked from large to small: EDTA-2Na > BQ > IPA. Therefore, ·OH, h^+, $\cdot O_2^-$ were all active substances involved in the degradation process.

By theoretically calculating the conduction band, valence band position, and free radical trapping experiments, the photocatalysis principle can be further analyzed. The results are shown in Fig. 10. Because the conduction band of Cu_2O is more negative than MoS_2 (about 0.52 eV), so when the light illuminates the surface of the semiconductor, Cu_2O is guided. The electrons on the belt are transferred to the MoS_2 conduction band, which also inhibits the recombination of photogenerated electrons and holes. The electrons on the MoS_2 conduction band rapidly adsorb oxygen and reduce it to $\cdot O_2^-$, which can react with water to form ·OH, which together act to decompose the organic dye molecules. h^+ migrated from the valence band of MoS_2 to the valence band of Cu_2O, and h^+ accumulated on the valence band also participated in the decomposition of organic pollutants. Therefore, the effective photodegradation of organic dyes using Cu_2O/MoS_2 can proceed smoothly, and the process can be summarized as:

$$Cu_2O/MoS_2 + hv \rightarrow (Cu_2O/MoS_2)^* + e^- + h^+ \quad (6)$$

$$O_2 + H_2O \rightarrow \cdot O_2^- \quad (7)$$

$$h^+ + MO \rightarrow \text{Oxide products} \quad (8)$$

$$O_2^- + H_2O \rightarrow H_2O_2 + \cdot OH \quad (9)$$

$$MO + h^+ / \cdot O_2^- / \cdot OH \rightarrow \text{Degraded products} \quad (10)$$

Conclusions

In summary, the novel nanocomposite CM-12 was synthesized by a simple two-step method, and the photocatalytic properties were studied. The results show that CM-12 can completely degrade MO in 30 min (degradation rate 91%) degradation. The pseudo-first-order kinetic constant is 8.76 times that of pure Cu_2O due to the decrease in photogenerated electron-hole recombination rate, and the material has good stability. After repeated use for 5 times, the degradation rate can still reach 40%. Through experimental and theoretical results, a possible photocatalytic mechanism is proposed, which is helpful to develop new photocatalysts and improve the catalytic performance of traditional photocatalysts.

Funding This study was funded by the National Natural Science Foundation of China (grant numbers 51572130, 51672134, and 51572127).

Compliance with ethical standards

Conflict of interest The authors declare that they have no conflict of interest.

References

1. Tripathy N, Ahmad R, Eun Song J, Ah Ko H, Hahn Y-B, Khang G (2014) Photocatalytic degradation of methyl orange dye by ZnO nanoneedle under UV irradiation. Mater Lett 136:171–174. https://doi.org/10.1016/j.matlet.2014.08.064
2. Yuan Q, Chen L, Xiong M, He J, Luo S-L, Au C-T, Yin S-F (2014) Cu2O/BiVO4 heterostructures: synthesis and application in simultaneous photocatalytic oxidation of organic dyes and reduction of Cr(VI) under visible light. Chem Eng J 255:394–402. https://doi.org/10.1016/j.cej.2014.06.031
3. Mao S, Bao R, Fang D, Yi J (2019) Fabrication of sliver/graphitic carbon nitride photocatalyst with enhanced visible-light photocatalytic efficiency through ultrasonic spray atomization. J Colloid Interface Sci 538:15–24. https://doi.org/10.1016/j.jcis.2018.11.078
4. Wen X-J, Shen C-H, Fei Z-H, Fang D, Liu Z-T, Dai J-T, Niu C-G (2020) Recent developments on AgI based heterojunction photocatalytic systems in photocatalytic application. Chem Eng J 383:123083. https://doi.org/10.1016/j.cej.2019.123083
5. Chong MN, Jin B, Chow CWK, Saint C (2010) Recent developments in photocatalytic water treatment technology: a review. Water Res 44(10):2997–3027. https://doi.org/10.1016/j.watres.2010.02.039
6. Wen X-J, Qian L, Lv X-X, Sun J, Guo J, Fei Z-H, Niu C-G (2020) Photocatalytic degradation of sulfamethazine using a direct Z-Scheme AgI/Bi4V2O11 photocatalyst: mineralization activity, degradation pathways and promoted charge separation mechanism. J Hazard Mater 385:121508. doi:https://doi.org/10.1016/j.jhazmat.2019.121508
7. Shen C-H, Wen X-J, Fei Z-H, Liu Z-T, Mu Q-M (2020) Visible-light-driven activation of peroxymonosulfate for accelerating ciprofloxacin degradation using CeO2/Co3O4 p-n heterojunction photocatalysts. Chem Eng J 391:123612. https://doi.org/10.1016/j.cej.2019.123612
8. Wu X, Zhang D, Jiao F, Wang S (2016) Visible-light-driven photodegradation of Methyl Orange using Cu2O/ZnAl calcined layered double hydroxides as photocatalysts. Colloids Surf Physicochem Eng Aspects 508:110–116. https://doi.org/10.1016/j.colsurfa.2016.08.047
9. Khataee A, Kalderis D, Gholami P, Fazli A, Moschogiannaki M, Binas V, Lykaki M, Konsolakis M (2019) Cu2O-CuO@biochar composite: synthesis, characterization and its efficient photocatalytic performance. Appl Surf Sci 498:143846. https://doi.org/10.1016/j.apsusc.2019.143846

10. Huang W-C, Lyu L-M, Yang Y-C, Huang MH (2012) Synthesis of Cu2O nanocrystals from cubic to rhombic dodecahedral structures and their comparative photocatalytic activity. J Am Chem Soc 134 (2):1261–1267. doi:https://doi.org/10.1021/ja209662v
11. Xu H, Wang W, Zhu W (2006) Shape evolution and size-controllable synthesis of Cu2O octahedra and their morphology-dependent photocatalytic properties. J Phys Chem B 110 (28): 13829–13834. doi:https://doi.org/10.1021/jp061934y
12. Zhang Y, Deng B, Zhang T, Gao D, Xu A-W (2010) Shape effects of Cu2O polyhedral microcrystals on photocatalytic activity. J Phys Chem C 114(11):5073–5079. https://doi.org/10.1021/jp9110037
13. Xu C, Cao L, Su G, Liu W, Liu H, Yu Y, Qu X (2010) Preparation of ZnO/Cu2O compound photocatalyst and application in treating organic dyes. J Hazard Mater 176(1):807–813. https://doi.org/10.1016/j.jhazmat.2009.11.106
14. Ma J, Wang K, Li L, Zhang T, Kong Y, Komarneni S (2015) Visible-light photocatalytic decolorization of Orange II on Cu2O/ZnO nanocomposites. Ceram Int 41 (2, Part A):2050-2056. https://doi.org/10.1016/j.ceramint.2014.09.137
15. Hu S, Zhou F, Wang L, Zhang J (2011) Preparation of Cu2O/CeO2 heterojunction photocatalyst for the degradation of Acid Orange 7 under visible light irradiation. Catal Commun 12 (9):794–797. doi: https://doi.org/10.1016/j.catcom.2011.01.027
16. Xu Y-h, Liang D-h, Liu M-l, Liu D-z (2008) Preparation and characterization of Cu2O–TiO2: efficient photocatalytic degradation of methylene blue. Mater Res Bull 43 (12):3474–3482. doi:https://doi.org/10.1016/j.materresbull.2008.01.026
17. Li Z, Meng X, Zhang Z (2018) Recent development on MoS2-based photocatalysis: a review. J Photochem Photobiol C: Photochem Rev 35:39–55. doi:https://doi.org/10.1016/j.jphotochemrev.2017.12.002
18. Yan H, Liu L, Wang R, Zhu W, Ren X, Luo L, Zhang X, Luo S, Ai X, Wang J (2020) Binary composite MoS2/TiO2 nanotube arrays as a recyclable and efficient photocatalyst for solar water disinfection. Chem Eng J 401:126052. https://doi.org/10.1016/j.cej.2020.126052
19. Zhao W, Liu Y, Wei Z, Yang S, He H, Sun C (2016) Fabrication of a novel p–n heterojunction photocatalyst n-BiVO4@p-MoS2 with core–shell structure and its excellent visible-light photocatalytic reduction and oxidation activities. Appl Catal B Environ 185: 242–252. https://doi.org/10.1016/j.apcatb.2015.12.023
20. Yuan Y, Shen P, Li Q, Chen G, Zhang H, Zhu L, Zou B, Liu B (2017) Excellent photocatalytic performance of few-layer MoS2/graphene hybrids. J Alloys Compd 700:12–17. https://doi.org/10.1016/j.jallcom.2017.01.027
21. Li J, Liu E, Ma Y, Hu X, Wan J, Sun L, Fan J (2016) Synthesis of MoS2/g-C3N4 nanosheets as 2D heterojunction photocatalysts with enhanced visible light activity. Appl Surf Sci 364:694–702. https://doi.org/10.1016/j.apsusc.2015.12.236
22. Zhang X, Shao C, Li X, Miao F, Wang K, Lu N, Liu Y (2016) 3D MoS2 nanosheet/TiO2 nanofiber heterostructures with enhanced photocatalytic activity under UV irradiation. J Alloys Compd 686: 137–144. https://doi.org/10.1016/j.jallcom.2016.05.336
23. Tan Y-H, Yu K, Li J-Z, Fu H, Zhu Z-QJJoAP (2014) MoS2@ ZnO nano-heterojunctions with enhanced photocatalysis and field emission properties. 116 (6):064305. https://doi.org/10.1063/1.4893020
24. Xi Q, Gao G, Jin M, Zhang Y, Zhou H, Wu C, Zhao Y, Wang L, Guo P, Xu J (2019) Design of graphitic carbon nitride supported Ag–Cu2O composites with hierarchical structures for enhanced photocatalytic properties. Appl Surf Sci 471:714–725. https://doi.org/10.1016/j.apsusc.2018.12.033
25. Meng X, Li Z, Zeng H, Chen J, Zhang Z (2017) MoS2 quantum dots-interspersed Bi2WO6 heterostructures for visible light-induced detoxification and disinfection. Appl Catal B Environ 210:160–172. https://doi.org/10.1016/j.apcatb.2017.02.083
26. Zuo S, Xu H, Liao W, Yuan X, Sun L, Li Q, Zan J, Li D, Xia D (2018) Molten-salt synthesis of g-C3N4-Cu2O heterojunctions with highly enhanced photocatalytic performance. Colloids Surf Physicochem Eng Aspects 546:307–315. https://doi.org/10.1016/j.colsurfa.2018.03.013
27. Zhang P, Wang T, Zeng H (2017) Design of Cu-Cu2O/g-C3N4 nanocomponent photocatalysts for hydrogen evolution under visible light irradiation using water-soluble Erythrosin B dye sensitization. Appl Surf Sci 391:404–414. https://doi.org/10.1016/j.apsusc.2016.05.162
28. He J, Shao DW, Zheng LC, Zheng LJ, Feng DQ, Xu JP, Zhang XH, Wang WC, Wang WH, Lu F, Dong H, Cheng YH, Liu H, Zheng RK (2017) Construction of Z-scheme Cu2O/Cu/AgBr/Ag photocatalyst with enhanced photocatalytic activity and stability under visible light. Appl Catal B Environ 203:917–926. https://doi.org/10.1016/j.apcatb.2016.10.086
29. Gong H, Zhang Y, Cao Y, Luo M, Feng Z, Yang W, Liu K, Cao H, Yan H (2018) Pt@Cu2O/WO3 composite photocatalyst for enhanced photocatalytic water oxidation performance. Appl Catal B Environ 237:309–317. https://doi.org/10.1016/j.apcatb.2018.05.086
30. Liu L, Qi Y, Hu J, Liang Y, Cui W (2015) Efficient visible-light photocatalytic hydrogen evolution and enhanced photostability of core@shell Cu2O@g-C3N4 octahedra. Appl Surf Sci 351:1146–1154. https://doi.org/10.1016/j.apsusc.2015.06.119
31. Xiong T, Wen M, Dong F, Yu J, Han L, Lei B, Zhang Y, Tang X, Zang Z (2016) Three dimensional Z-scheme (BiO)2CO3/MoS2 with enhanced visible light photocatalytic NO removal. Appl Catal B Environ 199:87–95. https://doi.org/10.1016/j.apcatb.2016.06.032
32. Liu G, Cui J, Luo R, Liu Y, Huang X, Wu N, Jin X, Chen H, Tang S, Kim J-K, Liu X (2019) 2D MoS2 grown on biomass-based hollow carbon fibers for energy storage. Appl Surf Sci 469:854–863. https://doi.org/10.1016/j.apsusc.2018.11.067
33. Yuan Y-J, Shen Z, Wu S, Su Y, Pei L, Ji Z, Ding M, Bai W, Chen Y, Yu Z-T, Zou Z (2019) Liquid exfoliation of g-C3N4 nanosheets to construct 2D-2D MoS2/g-C3N4 photocatalyst for enhanced photocatalytic H2 production activity. Appl Catal B Environ 246:120–128. https://doi.org/10.1016/j.apcatb.2019.01.043
34. Shi Y, Yang Z, Wang B, An H, Chen Z, Cui H (2016) Adsorption and photocatalytic degradation of tetracycline hydrochloride using a palygorskite-supported Cu2O–TiO2 composite. Appl Clay Sci 119:311–320. https://doi.org/10.1016/j.clay.2015.10.033
35. Ge L, Han C, Liu J (2011) Novel visible light-induced g-C3N4/Bi2WO6 composite photocatalysts for efficient degradation of methyl orange. Appl Catal B Environ 108-109:100–107. https://doi.org/10.1016/j.apcatb.2011.08.014
36. Han C, Ge L, Chen C, Li Y, Xiao X, Zhang Y, Guo L (2014) Novel visible light induced Co3O4-g-C3N4 heterojunction photocatalysts for efficient degradation of methyl orange. Appl Catal B Environ 147:546–553. https://doi.org/10.1016/j.apcatb.2013.09.038
37. Cao J, Luo B, Lin H, Xu B, Chen S (2012) Visible light photocatalytic activity enhancement and mechanism of AgBr/Ag3PO4 hybrids for degradation of methyl orange. J Hazard Mater 217-218: 107–115. https://doi.org/10.1016/j.jhazmat.2012.03.002
38. Shan R, Lu L, Gu J, Zhang Y, Yuan H, Chen Y, Luo B (2020) Photocatalytic degradation of methyl orange by Ag/TiO2/biochar composite catalysts in aqueous solutions. Mater Sci Semicond Process 114:105088. https://doi.org/10.1016/j.mssp.2020.105088
39. Zhang W, Xiao X, Zheng L, Wan C (2015) Fabrication of TiO2/MoS2@zeolite photocatalyst and its photocatalytic activity for degradation of methyl orange under visible light. Appl Surf Sci 358:468–478. https://doi.org/10.1016/j.apsusc.2015.08.054
40. Liu X, Xing Z, Zhang Y, Li Z, Wu X, Tan S, Yu X, Zhu Q, Zhou W (2017) Fabrication of 3D flower-like black N-TiO2-x@MoS2 for unprecedented-high visible-light-driven photocatalytic performance. Appl Catal B Environ 201:119–127. https://doi.org/10.1016/j.apcatb.2016.08.031

41. Cao C, Xiao L, Chen C, Cao Q (2015) Synthesis of novel Cu2O/BiOCl heterojunction nanocomposites and their enhanced photocatalytic activity under visible light. Appl Surf Sci 357:1171–1179. https://doi.org/10.1016/j.apsusc.2015.09.121
42. Wang D, Xu Y, Sun F, Zhang Q, Wang P, Wang X (2016) Enhanced photocatalytic activity of TiO2 under sunlight by MoS2 nanodots modification. Appl Surf Sci 377:221–227. https://doi.org/10.1016/j.apsusc.2016.03.146
43. Song Y, Lei Y, Xu H, Wang C, Yan J, Zhao H, Xu Y, Xia J, Yin S, Li H (2015) Synthesis of few-layer MoS2 nanosheet-loaded Ag3PO4 for enhanced photocatalytic activity. DTr 44(7):3057–3066. https://doi.org/10.1039/C4DT03242J
44. Liqiang J, Yichun Q, Baiqi W, Shudan L, Baojiang J, Libin Y, Wei F, Honggang F, Jiazhong S (2006) Review of photoluminescence performance of nano-sized semiconductor materials and its relationships with photocatalytic activity. Sol Energy Mater Sol Cells 90(12):1773–1787. https://doi.org/10.1016/j.solmat.2005.11.007
45. Huang T, Lin X, Xing J, Wang W, Shan Z, Huang F (2007) Photocatalytic activities of hetero-junction semiconductors WO3/SrNb2O6. Mater Sci Eng B 141(1):49–54. https://doi.org/10.1016/j.mseb.2007.05.007
46. Wen X-J, Niu C-G, Zhang L, Liang C, Guo H, Zeng G-M (2018) Photocatalytic degradation of ciprofloxacin by a novel Z-scheme CeO2–Ag/AgBr photocatalyst: influencing factors, possible degradation pathways, and mechanism insight. J Catal 358:141–154. doi: https://doi.org/10.1016/j.jcat.2017.11.029
47. Wen X-J, Niu C-G, Zhang L, Liang C, Zeng G-M (2018) A novel Ag2O/CeO2 heterojunction photocatalysts for photocatalytic degradation of enrofloxacin: possible degradation pathways, mineralization activity and an in depth mechanism insight. Appl Catal B Environ 221:701–714. https://doi.org/10.1016/j.apcatb.2017.09.060
48. Wu Y, Wang H, Tu W, Liu Y, Wu S, Tan YZ, Chew JW (2018) Construction of hierarchical 2D-2D Zn3In2S6/fluorinated polymeric carbon nitride nanosheets photocatalyst for boosting photocatalytic degradation and hydrogen production performance. Appl Catal B Environ 233:58–69. https://doi.org/10.1016/j.apcatb.2018.03.105